IEEE Access
Multidisciplinary | Rapid Review | Open Access Journal

Received November 22, 2018, accepted December 20, 2018, date of publication January 1, 2019, date of current version January 29, 2019.

Digital Object Identifier 10.1109/ACCESS.2018.2890542

Analysing the Dynamics of Interbeat Interval Time Series Using Grouped Horizontal Visibility Graph

GULRAIZ IQBAL CHOUDHARY[1], WAJID AZIZ[2,3], ISHTIAQ RASOOL KHAN[2], SUSANTO RAHARDJA[4], (Fellow, IEEE), AND PASI FRÄNTI[1], (Senior Member, IEEE)

[1]School of Computing, University of Eastern Finland, 80101 Joensuu, Finland
[2]Faculty of Computing and Information Technology, University of Jeddah, Ash Sharafiyah 21589, Saudi Arabia
[3]Department of Computer Science, University of Azad Jammu & Kashmir, Muzafarabad 13100, Pakistan
[4]School of Marine Science and Technology, Northwestern Polytechnical University, Xi'an 710072, China

Corresponding author: Susanto Rahardja (susantorahardja@ieee.org)

This work was supported by the Lockheed Martin and King Abdulaziz City for Science and Technology (KACST). The work of S. Rahardja was supported in part by the 111 Project under Grant B18041.

ABSTRACT Horizontal visibility graph (HVG) motifs have been recently introduced to analyze the dynamical information encoded by biological signals. However, the result of the analysis strongly depends on the selected window size of the motifs. Different sizes ranging from 3 to 5 have been previously used, but such small window sizes are insufficient to cope with the complexity of biological systems and often fail to extract salient features of the encoded information. It is known that larger window size increases the total number of possible motifs, and it leads to the distribution of the statistics into too many motifs, which causes each individual motif to contain too little information and make it even more difficult to reliably detect system dynamics. To resolve this problem, we group the motifs based on the number of edges. Using the grouped motifs, we propose grouped horizontal visibility entropy (GHVE) to quantify the complexity based on the probability distribution of the observations within these groups. We apply GHVE to quantify the complexity of simulated white and 1/f noise. The results reveal that the 1/f noise time series exhibits a higher complexity than white noise time series, which indicates that the 1/f noise is structurally more complex than white Gaussian noise. We apply the method for analyzing interbeat intervals time series. The results show that the proposed GHVE measure is more accurate in distinguishing healthy and pathological subjects than its non-grouped counter-part HVG. It is, therefore, better suited to detect changes in aging, disease severity, and activity levels (sleep and wake period).

INDEX TERMS Complex network, HVG motifs, HRV analysis, time series data.

I. INTRODUCTION

The mapping of time series onto complex networks (graphs) [1], [2] has attained considerable attention in a variety of fields. It has been applied in the analysis of financial time series [1], stock market empirical record [2], *electroencephalography* (EEG) [3], [4], and *interbeat interval* (IBI) time series [5], [6]. Complex networks opened up new possibilities to quantify the dynamics of any time series by describing the structure at different temporal scales ranging from microscopic to macroscopic levels [2]. A complex network interprets the system components as nodes and their interaction as edges [7], [8], which provides a mechanism to characterize the complexity of the time series from a novel prospective. Complex network analysis has been applied in diverse research areas such as financial time series [1], [9], turbulence [10], and cardiac IBI time series [11]–[14].

Zhang and Small [11] pioneered the construction of complex networks from pseudo-periodic time series, where each cycle was represented by a single node in the network. They investigated the statistical properties of the constructed networks and found that time series with different dynamics exhibit distinct topological structures. Yang and Yang [12] constructed networks by dividing the time series into different segments to determine edges between the nodes in terms of the Pearson correlation coefficient. Gao and Jin [15] and Gao *et al.* [16] proposed a similar approach to construct networks from experimental flow signals. They employed network motifs to quantify the nonlinear characteristics of the

two-phase flow. The approach uses high value of embedding dimension to compute the correlation coefficient with low uncertainty and without the local short-term dynamics, but resulting in the loss of dynamical information [17].

Visibility graph (VG) is another method that has been used for efficient construction of networks from a time series [18]. Many VG algorithms have been developed and successfully applied both to EEG [3], [4] and IBI time series [5]. However, this approach transforms the time series into a static network which makes it difficult to extract dynamic behavior of the system. Luque *et al.* [19] developed an algorithm to construct horizontal visibility graph (HVG), which is a geometrically simpler and more efficient subgraph of VG than the full VG. The algorithm and the results presented in [19] are suitable for distinguishing uncorrelated randomness from chaos. Both VG and HVG have the ability to encode information of the time series structure and its underlying dynamics [1]. In previous studies [19], [29], window sizes between 3 and 5 were used to compute the probability of occurrence of HVG motifs, and HVG entropy (HVE) was then used to quantify the dynamical information. However, since physiological systems contain structures at multiple time scales, smaller window sizes are not reliable to extract subtle information about the system dynamics. This is because non-visibility motifs are more dominant than visibility motifs. Larger window sizes result in a significant increase in the number of motifs. For example, the number of distinct motifs increases from 22 to approximately 7,000 when increasing the window size from 5 to 10. However, many motifs produced by a larger window contain very little information about the system dynamics. The selection of the optimal window size remains an unresolved problem.

In this work, we compute the probability of occurrence of the grouped motifs to determine dynamical characteristics of a network motif system. The number of HVG motifs depends on the window size, i.e., the number of nodes involved in an HVG. We use a large window size to generate large number of distinctive motifs. However, these motifs are then grouped based on their structural symmetries. This keeps their probability distribution more uniform across the motif groups and allows more accurate analysis. We propose to use *grouped HVG entropy* (GHVE) to compute the dynamical information. GHVE provides information about short-term dynamical fluctuations that plays an integral role for the detection of age- or disease-related changes. We experimentally vary the window size between 3 and 15 nodes. (Please note that increasing the window size beyond 15 would lead to large number of motifs having little or no information with zero probability of occurrence.) Our findings indicate that a larger window size of 15 provides better separation between healthy and pathological subjects as compare to smaller windows.

The performance of GHVE is evaluated both using simulated noise signals and IBI time series data from real subjects with the conditions: *normal sinus rhythm* (NSR), *congestive heart failure* (CHF), and *atrial fibrillation* (AF) [20]. We determine the optimal window size for studying the long- and short-term visibility of the constructed network. A machine learning technique is used to classify the time series data into healthy or pathological based on GHVE features and identify the condition (NSR, CHF, or AF). The results reveal that features extracted using grouped HVG are good enough for machine learning models to be able to identify a signal either as NSR, CHF, or AF subjects. Finally, we compared GHVE against three existing techniques: sample entropy [21], permutation entropy [22], and bubble entropy [23]. The comparison indicates that the GHVE algorithm is more robust to reveal dynamically accurate information and provides the best degree of separation between healthy and pathological subjects.

II. MATERIAL AND METHODS

A. HVG MOTIFS

VG algorithms map time series data to a graph in order to explore the structure and underlying system dynamics. For a time series $\{t(i)\}_{i=1}^{N}$ comprising N data points, VG is a planar graph of N nodes in which every data point $t(i)$ is mapped to a node i, and two nodes i and j are connected by an edge if every data point $t(k)$ in between $t(i)$ and $t(j)$ fulfils the following criterion of convexity [18]

$$t_k < t_i + \frac{k-i}{j-i}\left[t_j - t_i\right] \quad \forall k : i < k < j. \tag{1}$$

In case of HVG, the time series is mapped to the graph such that every data point $t(i)$ is mapped to a node i, and two nodes, i and j, are connected by an edge if every point $t(k)$ in between $t(i)$ and $t(j)$ fulfils the following convexity criterion [19]

$$t_k < max\left(t_i, t_j\right) \quad \forall k : i < k < j. \tag{2}$$

An HVG can be broken into a set of uniquely defined subgraphs called motifs. Each motif represents some topological properties of the graph including the information about data relation and temporal ordering in the structure [24]. Fig. 1 illustrates the schematic transformation of an IBI time series into an HVG.

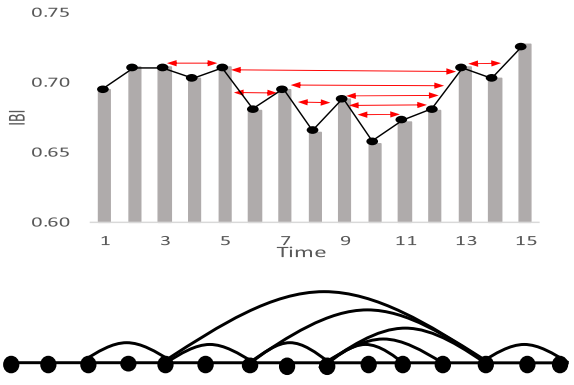

FIGURE 1. Horizontal visibility indicated by arrows of time series data of 15 points (top), and the extracted HVG (bottom).

HVG motifs are outerplanar, i.e., their edges do not intersect (Fig. 2). The total number of n-node HVG motifs associated with a time series having N data points is $M = N - n$.

FIGURE 2. Example of an outerplanar motif where edges do not intersect (left) and the non-outerplanar alternative (right). HVG motifs are outerplanar.

An n-node motif can have various configurations. For a 5-node HVG, a total of 22 admissible outerplanar motifs exist (Table I). If the total number of motifs in a window of n-nodes is M, then a probability vector P^n can be constructed as

$$P^n : n \in N \left[p_1^n, p_2^n, \ldots\ldots p_M^n\right] \in [0,1]^M , \tag{3}$$

where p_i^n is the probability of occurrence of the i^{th} motif in the graph. The dynamics of the underlying system can be quantified by calculating the entropy of HVG using the Shannon entropy [25], as

$$HVE_n = \sum P_i^n \log P_i^n. \tag{4}$$

B. GROUPED HVG MOTIFS

Since real data (IBI time series) shows structures at multiple temporal scales, smaller windows are unable to accurately capture the system dynamics. While increasing the window size increases the number of motif types, it also decreases the information contained in each type. To address this issue, instead of computing the probability of occurrence of each motif type, we compute the probability of occurrence of a group of motifs that have the same number of edges. For example, the 22 HVG motifs for size $n = 5$ nodes shown in Table I can be divided into four groups, g_{0-3}, where the subscript gives the number of edges present in a motif (g_0 thus corresponds to no visibility, g_1 to one edge, etc.). If M_g is the total number of groups labelled from 0 to $M_g - 1$, then the n-node HVG motif profile P_g^n for a time series having N data points can be written as

$$P_g^n : n \in N \left[p_{g0}^n, p_{g1}^n, \ldots\ldots p_{Mg}^n\right] \in [0,1]^{Mg} . \tag{5}$$

Note that Eq. (5) differs from Eq. (3) in that it calculates the probability of occurrence of a group of motifs and not individual motif. After calculating the probability vector in Eq. (5), the Shannon entropy [25] can be used to quantify the dynamics of the system as

$$GHVE_n = \sum P_{gi}^n \log P_{gi}^n. \tag{6}$$

TABLE 1. Possible horizontal visibility graph motifs of size n=5.

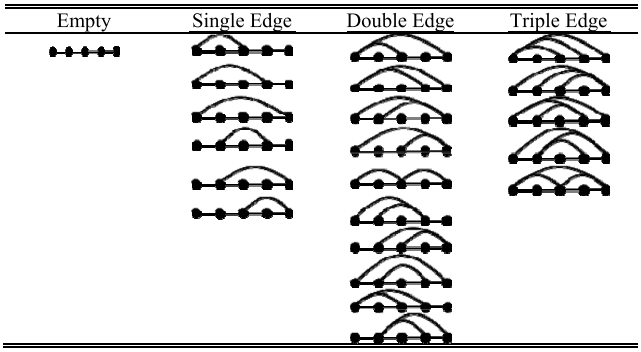

C. DATASET

We evaluated the performance of GHVE by using synthetic and clinical datasets. The synthetic data contains both *white Gaussian noise* (WGN) and $1/f$ noise. Both are commonly used in multiscale entropy analyses [26], [27]. WGN is randomly drawn from a Gaussian distribution and therefore it is statistically uncorrelated and has a constant power spectral density. For $1/f$ noise, the power spectral density is inversely proportional to the frequency (hence the name $1/f$) and is equal to the amount of energy octave [28]. For generating $1/f$ noise, we start with uniformly distributed white noise and calculate its *fast Fourier transform* (FFT). The $1/f$ distribution is then imposed on the power spectrum before calculating the inverse FFT [29]. For our experiments, we generate 40 datasets in total, each of which consists of 40,000 data points.

The clinical data used in this study consists of several IBI time series datasets taken from Physionet (www.physionet.org), which is a well-known resource for research on complex physiological signals [30]. The data consists of 72 NSR, 44 CHF, and 24 AF subjects (Table II). The NSR datasets were obtained from 24-hour holter monitor recordings. Out of 72 NSR subjects, 54 were taken from the RR-interval normal sinus rhythm database and 18 from the MIT-BIH normal sinus rhythm database [30]. There was a total of 35 men and 37 women, aged between 20-78 years (mean $\pm$1STD $= 54.6 \pm 16.2$ years). All recordings in the NSR dataset were sampled at 128 Hz [30].

TABLE 2. Inter BEAT interval time series data for healthy and pathological subjects.

	NSR	CHF	AF
Total Subjects	72	44	24
Gender	35 M 37 F	29 M 15 F	Unknown
Age Group	20-78	20-78	20-78
Recorder	24 hr Holter Monitor	24 hr Holter Monitor	10 hr Ambulating ECG Recorder
Sampling	R-R 128 Hz	29 R-R 128 Hz 15 MIT BIH 250 Hz	250 Hz

The time series data of the 44 CHF subjects was also obtained from 24-hour holter monitor recordings. 29 of which originate from the RR-interval congestive heart failure database (128Hz sampling frequency). The remaining 15 are taken from the MIT-BIH Bidmic congestive heart failure database (250 Hz sampling frequency). According to the *New York Heart Association* (NYHA) functional classification system, CHF subjects are typically divided into four classes [31] based on a patient's ability to perform physical

activity. While patients in Class I do not experience any discomfort when carrying out physical activities, the discomfort increases for Classes II to IV with the latter being unable to carry out any physical activity at all without experiencing discomfort (severe disease category).

In this paper, CHF subjects are divided into two categories. The first group, CHFA (less severe), consists of 12 subjects with lesser disease severity from NYHA Classes I and II. The second group, CHFB (more severe), consists of 32 subjects with high disease severity ordinarily classified into NYHA Classes III and IV.

AF data used in our study has been taken from the MIT-BIH Atrial Fibrillation database (AFDB) [30] and comprises the RR-interval time series data of 24 AF subjects. Individual recordings have a duration of 10 hours. The original analogue signals were recorded using ambulatory ECG recorders with a typical recording bandwidth of approximately 0.1 Hz to 40 Hz and sampling frequency of 250 Hz [30].

D. STATISTICAL ANALYSIS

Analysis of variance (ANOVA) is generally used to analyze differences among group means and their concomitant measures for three or more groups. One-way ANOVA is an omnibus test based on significant F statistics, which determines whether the group means differ in a statistically significant manner. However, ANOVA does not make paired comparisons but only determines whether a group is significantly different from the rest. We use ANOVA for analysis of the difference among group means and the Bonferroni post-hoc test for multiple comparisons among the groups.

Our feature set is comprised of GHVE estimates computed using Eq. (6) for each motif group using a sliding window consisting of 15 nodes using time series data of *NSR young* (NSRY), CHF, and AF subjects. *Support vector machine* (SVM), *k-nearest neighbors* (kNN), *Random tree* (RT), and C4.5 (J48) classifiers are used, employing 10-fold cross-validation to evaluate the performance of classification models. A confusion matrix is constructed to visualize correct and incorrect predictions made by the classification algorithm with regard to the actual class labels in the dataset.

III. RESULTS

GHVE is applied to two simulated noise signals. The four possible motif groups for the 5-node window size are dominated by zero (no visibility) edge group, g_0, thus revealing very little structural information about the system dynamics (Fig. 3). The probability of occurrence of motif groups and their GHVE values almost overlap for WGN and 1/*f* noise signals, rendering both signals nearly indistinguishable. When the window size is increased to 10 and 15, the number of possible motif groups increases to 9 and 14, respectively, providing more structural information about the system dynamics. The increase in the window size thus results in the information being distributed among a larger number of motif groups. As this decreases the probability of occurrence of g_0, it provides better insights into the system dynamics. For larger window sizes, both the probability of occurrence of a motif group and the corresponding GHVE values are higher for 1/*f* noise than for WGN noise signals for g_0, g_1, and g_7 to g_{10} motif groups (Figs. 3 and 4). The opposite trend is observed for motif groups g_2 to g_6, while for motif groups g_{11} to g_{13}, the results are very similar. It follows that both noise signals can only be distinguished if many motif groups are present, i.e., for larger window sizes.

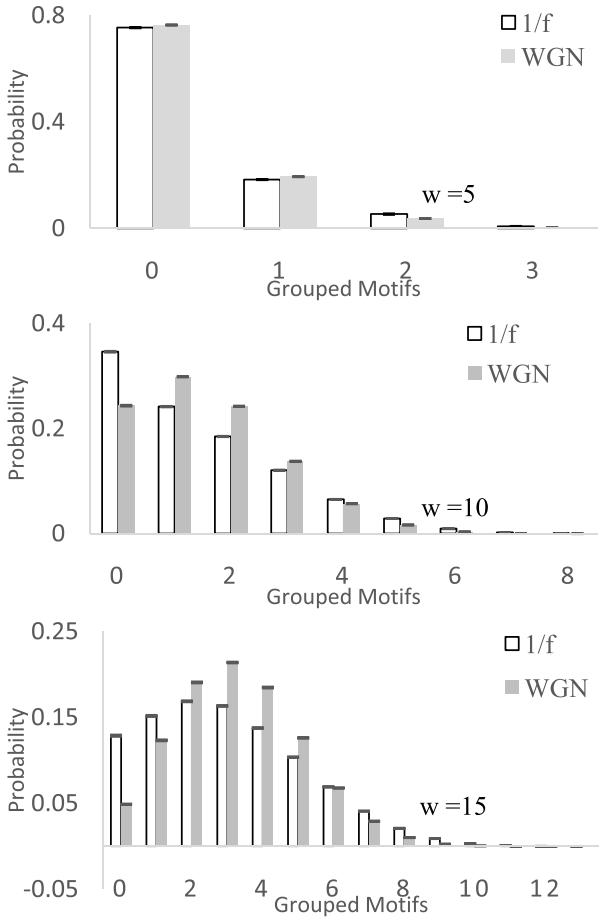

FIGURE 3. Probability of occurrence of group HVG motifs at widow sizes 5, 10, and 15 for synthetic data.

To test the suitability of GHVE for distinguishing between healthy and diseased subjects using real IBI time series data, we evaluated the performance of GHVE at different window sizes. Results were more accurate and robust using a window size with 15 nodes (Fig. 5). Compared to CHFB, the NSR GHVE values are higher for g_0 to g_4 motif groups and overlap for groups g_5 to g_7 and tend to overlap for groups g_8 to g_{13}. Compared to AF, the NSR GHVE values are higher for groups g_0 to g_7 and lower for the remaining groups. The higher NSR values show that the complexity of NSR subjects is higher than either CHFB (g_0 to g_4) or AF subjects (g_0 to g_7). When comparing CHFB and AF subjects, we found that CHFB subjects have higher GHVE values at g_0 to g_7 and lower values for the remaining groups.

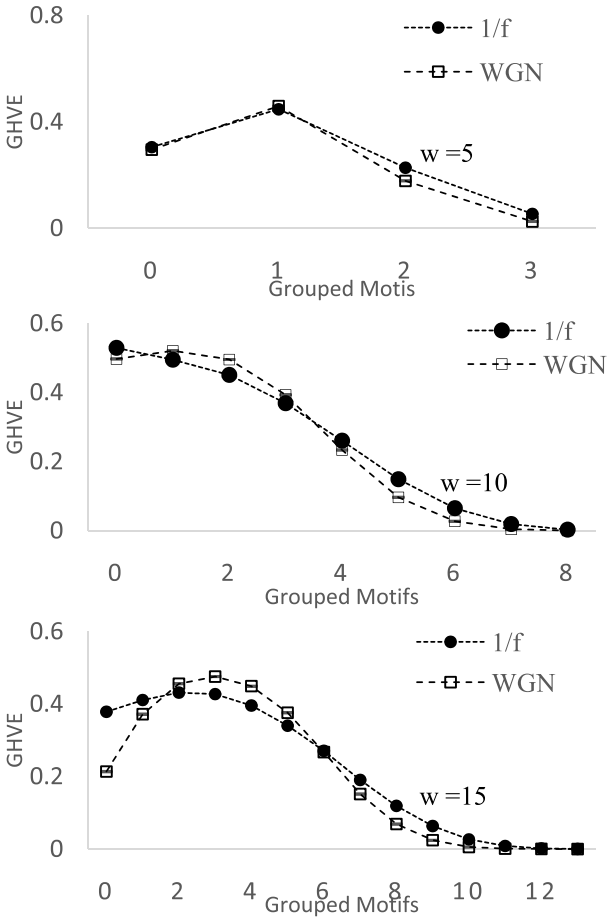

FIGURE 4. Mean ± SE of GHVE estimates for distinguishing synthetic data.

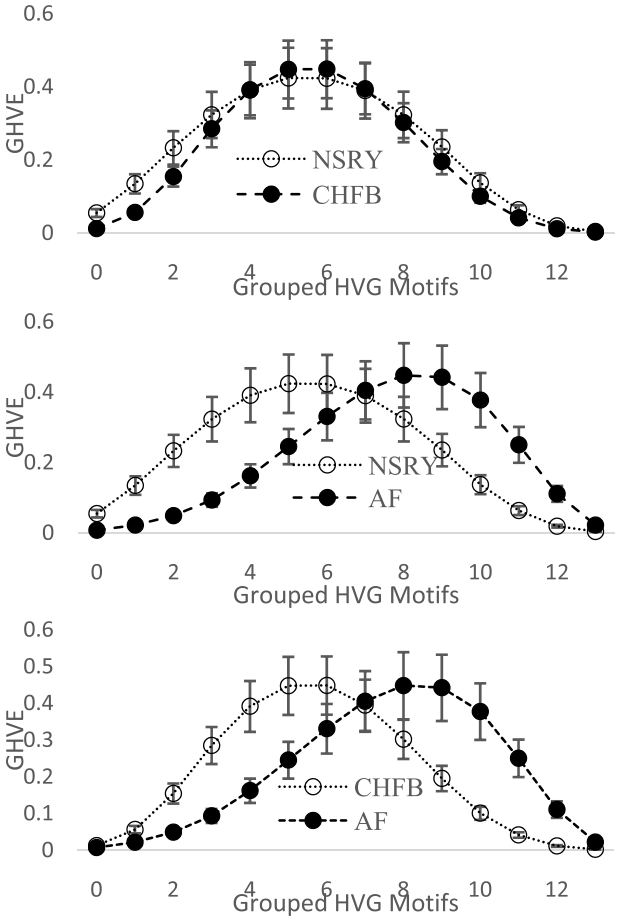

FIGURE 5. Mean ± SE of GHVE estimates at window size 15 for distinguishing clinical data. The circles represent mean values and error bars represent the standard error.

ANOVA is used to analyze the differences among group means and a Bonferroni post-hoc test is used for paired comparisons between NSRY vs CHF, NSRY vs AF, and CHF vs AF subjects. The p-value <0.05 is a level of significance difference between motif groups. GHVE values differed in a statistically significant manner for all pairs and across a wide range of motif groups. The maximum separation for each pairwise comparison was obtained at: g_1 for NSRY vs CHFB (p-value$=1.3\times10^{-06}$), g_4 for NSRY vs AF (p-value$=1.3\times10^{-14}$), and g_6 for CHFB vs AF (p-value$=5.2\times10^{-14}$). The increase in complexity explains why it is difficult to assess this dynamical behavior using traditional approaches on RR-interval time series data. The distribution of GHVE patterns in NSRY subjects is more uniform than in pathological (CHF, AF) and elderly subjects which leads to a larger GHVE value at a wide range of motif groups (Figs. 6 and 7). Furthermore, complexity clearly decreases with disease severity and age. These results are in good agreement with the ''loss of complexity with aging and disease'' hypothesis [26], [32], [33].

We evaluated the performance of GHVE to compare CHFA (low severity) with CHFB (high severity) subjects. GHVE values were higher for CHFA at motif groups g_0 to g_4 and g_9 to g_{13} and lower for g_5 to g_8. The maximum separation between CHFA and CHFB was obtained for g_0 (p-value$=0.0046$). GHVE values were higher for young vs elderly subjects and for low (CHFA) vs high (CHFB) disease severity. The decrease in GHVE reflects the loss of complexity with advanced age and disease severity.

We evaluated the performance of GHVE for characterizing the dynamics of NSRY and *NSR elderly* (NSRE) subjects and for investigating the changing dynamics with disease severity. It is evident that GHVE values are higher for NSRY at motif groups g_0 to g_2 and g_7 to g_{13}, and lower for g_3 to g_6 (Fig. 6). The maximum separation between the young and elderly subjects was obtained at motif group 13 (p-value $=3.7\times10^{-4}$).

To assess the effects of physical activity, we computed the complexity of the IBI time series for healthy subjects during their sleep and wake periods. From the 24-hour IBI time series data of 72 healthy subjects, the sleep/wake datasets were obtained by extracting 20,000 consecutive data points that showed the highest/lowest heart rate. Although GHVE can distinguish between sleep and wake data at motif groups g_3 to g_5 and g_7 to g_{11}, only groups g_7 to g_{11} provide

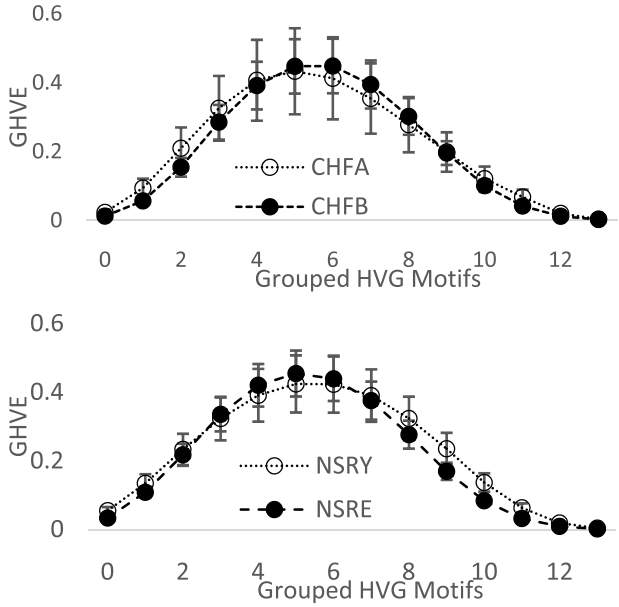

FIGURE 6. Mean ± SE of GHVE estimates at window size 15 for distinguishing the subjects-based on disease severity and aging.

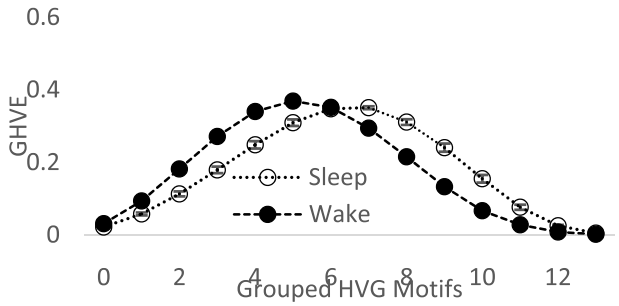

FIGURE 7. Mean ± SE of GHVE estimates at window size 15 for distinguishing sleep and wake periods.

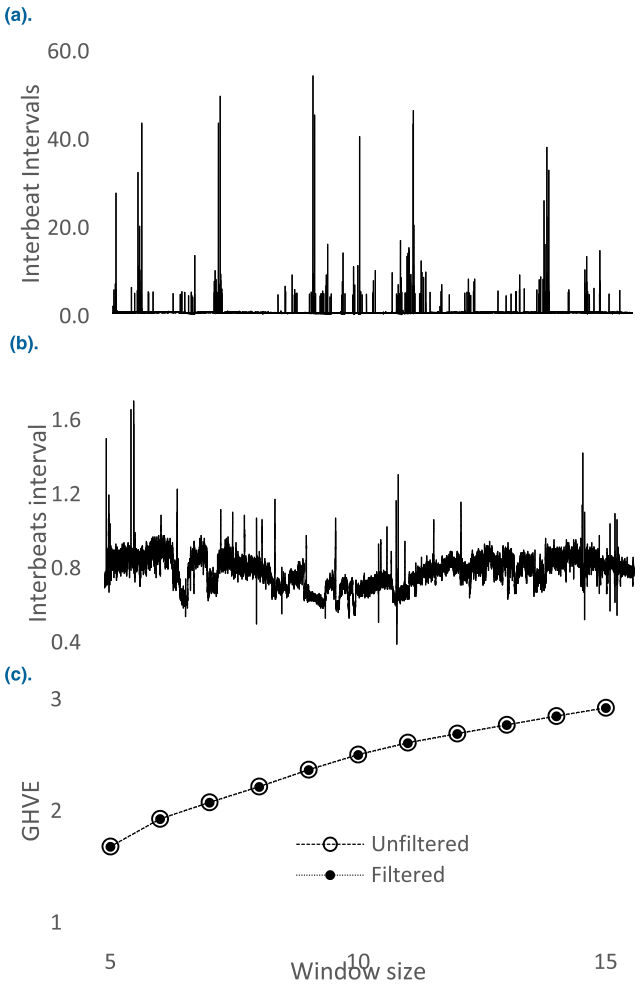

FIGURE 8. GHVE on interbeat interval time series of healthy subjects before and after removing artefacts greater than 2s.

dynamically correct information, i.e., higher values during sleep and smaller values when awake (Fig. 7). These results support the notion that the cardiac dynamics of healthy subjects are more complex under free-running conditions.

By applying GHVE to the IBI time series of the healthy subjects with and without outliers, where outliers are defined as having a value greater than 2 seconds, we observed a total of 30,000 data points whose absolute values were much higher than normal IBI intervals and therefore classified as outliers (Fig. 8a). Fig. 8 (b) shows the IBI time series after having removed artefacts with intervals greater than 2s. The GHVE curves of the filtered and unfiltered time series overlap, indicating that GHVE is still a robust method, even in the presence of a small percentage of high amplitude outliers (Fig. 8c).

By examining the classification accuracy (Table III), we find that all tested classifiers can easily classify NSR, CHF, and AF subjects using the proposed GHVE measure. The highest accuracy was obtained by the J48 algorithm.

We compared the GHVE with other entropy estimates in terms of dynamical information and their ability to discriminate different groups (Table IV). In accordance with the "loss of complexity with age and disease" hypothesis, healthy/young subjects exhibit higher complexity compared to pathological/elderly subjects [26], [32], [33]. The dynamical information is accurate if healthy/young subjects exhibit higher complexity and vice versa.

The more accurate dynamical information is provided by GHVE, followed by sample entropy, and finally bubble entropy. Although HVE and permutation entropy provided a better separation between NSR and AF subjects, the GHVE results are superior for two reasons: (1) HVE and permutation entropy provided dynamically inaccurate information suggesting a higher complexity for pathological/elderly subjects (thus violating the "loss of complexity with age and disease" hypothesis); (2) GHVE not only accurately distinguishes between NSRY and AF subjects but also provides a better separation between both NSRY and NSRE and NSRY and CHF subjects, while HVE and permutation entropy failed to do so.

TABLE 3. Classification Accuracy of different machine learning classifiers in Terms of True positive rate (TPR), False Positive rate (FPR), precision, recall, f-measure and area under roc (auc).

Class	TPR	FPR	Precision	Recall	F-Measure	AUC
			SVM			
NSR	0.57	0.01	0.93	0.57	0.71	0.82
CHF	0.93	0.24	0.71	0.93	0.81	0.84
AF	0.91	0.03	0.91	0.91	0.91	0.95
			KNN			
NSR	0.88	0.10	0.79	0.88	0.83	0.88
CHF	0.81	0.12	0.81	0.81	0.81	0.81
AF	0.75	0.05	0.85	0.75	0.80	0.85
			Random Tree			
NSR	0.88	0.03	0.92	0.88	0.90	0.92
CHF	0.90	0.06	0.90	0.90	0.90	0.92
AF	0.91	0.05	0.88	0.91	0.89	0.93
			J48			
NSR	0.96	0.03	0.92	0.92	0.94	0.94
CHF	0.90	0.00	1.00	0.90	0.95	0.92
AF	1.00	0.03	0.92	1.00	0.96	0.96

The smaller p-values and higher AUC provide evidence that GHVE possesses the highest discriminatory power to distinguish NSRY vs CHF (p-value=9.65×10^{-13}), NSRY vs AF (p-value=1.10×10^{-8}), and NSRY vs NSRE (p-value=6.27×10^{-7}). Bubble entropy showed a better separation between NSRY vs CHF (p-value=3.17×10^{-9}), followed by NSRY vs AF, but did not show a significant difference between NSRY vs NSRE (p-value=1.00). Sample entropy performed well in distinguishing NSRY vs CHF and NSRY vs NSRE but failed with NSRY vs AF. Permutation entropy failed to discriminate NSRY and CHF while successfully separating NSRY vs NSRE and NSRY vs AF. GHVE is the only HRV measure to provide dynamically accurate information about different healthy and pathological groups yielding the better overall classification results.

IV. DISCUSSION

In this paper, we introduced the concept of grouped HVG motifs to address the issue of small windows (providing lesser information) and to handle the information content generated by larger windows due to large increased in the number of motifs. By using GHVE to estimate the entropy of simulated WGN and $1/f$ noise, we could establish that smaller window sizes reveal less structural information compared to large window sizes. For smaller windows, the GHVE values almost overlap for WGN and $1/f$ noise signals making the two signals nearly indistinguishable. An increase in window size resulted in the distribution of information among a larger number of motif groups, thereby decreasing the probability of occurrence of zero visibility edges. GHVE values were higher for $1/f$ noise signals at wide range grouped motifs and the two noise signals become distinguishable. Higher GHVE values indicate that $1/f$ noise contains more complex structures, a result that is consistent with previous studies [27]. However, when employing GHVE one needs to consider the window size and use grouped motifs for a better characterization of complex signals.

We tested GHVE for its capacity to distinguish between time series data from healthy (NSR) and pathological (CHF and AF) subjects and identify age and disease severity-related changes. The results suggested that GHVE can successfully distinguish between healthy and diseased groups with J48 being the most accurate classifications. For CHF, the disease dynamics were associated with a loss of variability (emergence of regular patterns), whereas for AF, the disease dynamics results in a more random pattern. We found GHVE values to be higher for healthy compared to pathological subjects across a wide range of motif groups. GHVE values were smaller for elderly subjects and lower disease severity. Higher GHVE values indicate a higher dynamical complexity of the system. Our approach is in agreement with the "loss of complexity with age and disease" paradigm. This loss of complexity can be attributed to the decoupling or degradation of the cardiac autonomous control. Our study verified this hypothesis for NSR, CHF, and AF subjects as well as for elderly subjects. In a recent study by Manis *et al.* [23] using bubble entropy to quantify the dynamics of control and CHF subjects, they found that bubble entropy yielded incorrect

TABLE 4. Comparison of GHVE, bubble entropy, Sample Entropy and permutation entropy for distinguishing NSRY, NSRE, CHF and AF subjects. areas under ROC (AUC) for optimal separation between healthy, low disease severity and high disease severity (AUC = 0.5 is equivalent to simple guessing and AUC = 1 is equivalent to perfect separation between classes, P-VALUE shows significant difference at ≤0.05).

	Mean ± Standard Error				NSRY VS NSRE		NSRY VS CHF		NSRY VS AF	
	NSRY	NSRE	CHF	AF	p-value	AUC	p-value	AUC	p-value	AUC
GHVE	3.15 ±0.02	2.95 ±0.02	2.83 ±0.03	2.88 ±0.04	6.27×10^{-7}	0.89	9.65×10^{-13}	0.94	1.10×10^{-8}	0.91
HVE [34]	1.59 ±0.02	1.55 ± 0.02	1.59 ±0.01	1.77 ±0.01	0.75	0.62	1.00	0.51	3.43×10^{-10}	0.94
Bubble Entropy [23]	0.34 ±0.00	0.34 ±0.00	0.32 ±0.00	0.33 ±0.00	1.00	0.57	3.17×10^{-9}	0.89	0.01	0.77
Sample Entropy [24]	0.86 ±0.04	0.60 ±0.04	0.68 ±0.06	0.73 ±0.11	0.01	0.79	0.200	0.71	1.00	0.73
Permutation Entropy [25]	1.69 ±0.01	1.72 ±0.01	1.72 ±0.01	1.76 ±0.01	0.03	0.71	0.12	0.68	4.50×10^{-10}	0.93

dynamical information about control and CHF subjects for small embedding dimensions (<8), assigning a lower entropy to control compared to CHF subjects. For embedding dimensions >8, bubble entropy assigned higher entropies to control subjects compared to CHF, thus concurring with the "loss of complexity with age and disease" paradigm.

Our study provides new insights with regard to the dynamical information content and classification capabilities of GHVE. GHVE provided dynamically correct information about both simulated and real signals, while HVE failed to do so. The $1/f$ noise signals contain complex structures due to the presence of long-range correlations and are more complex than WGN. Higher GHVE values indicated that $1/f$ noise signals are dynamically more complex than WGN. The complexity of healthy biological systems reflects the ability to adapt and function in a dynamic environment. Aging and disease reduce the ability to adapt and function in a dynamic environment, resulting in a decrease in complexity. Our results demonstrate that healthy systems are dynamically more complex than pathological ones. From a classification perspective, GHVE was able to successfully separate $1/f$ and WGN signals. Compared to various entropy-based complexity measures, GHVE proved to be superior in distinguishing, NSRY vs NSRE, NSR vs CHF, and CHF vs AF subjects.

V. CONCLUSION

In this paper, we proposed GHVE to analyze the dynamics of biological systems exhibiting complex fluctuations. The performance of GHVE has been evaluated using simulated noise signals and IBI time series data from healthy and pathological subjects. We transformed the time series into HVG motifs and grouped them on the basis of number of edges. Then we computed the probability occurrence of grouped motifs and their entropy GHVE. The results showed that for smaller window sizes GHVE values for WGN and $1/f$ noise signals overlapped. $1/f$ noise had higher values across a wide range of motif groups compared to WGN revealing that correlated signals were more complex. The two signals become distinguishable once the window size was increased. The higher GHVE values for $1/f$ noise across a wide range of motif groups reveal that correlated signals ($1/f$) are more complex than uncorrelated signals (WGN). The results proved the effectiveness of our method for distinguishing and classifying IBI time series into healthy and pathological subjects and to identify changes due to aging and disease dynamics. Compared to other complexity measures, the GHVE algorithm showed more accurate dynamical information. It also provided the best separation between healthy and pathological subjects of varying severity. In addition, when compared with other competing methods, it exhibited superiority for identifying changes related to the subjects' activity level. Further possible applications include the dynamics of EEG signals for detecting epileptic and non-epileptic seizures, distinguishing focal and non-focal EEG signals, and characterizing dynamics of human unconstrained and metronomic walking protocols.

REFERENCES

[1] E. Zhuang, M. Small, and G. Feng, "Time series analysis of the developed financial markets' integration using visibility graphs," *Phys. A, Stat. Mech. Appl.*, vol. 410, pp. 483–495, Sep. 2014.
[2] M. Stephen, C. Gu, and H. Yang, "Visibility graph based time series analysis," *PLoS ONE*, vol. 10, no. 11, e0143015, 2015.
[3] M. Ahmadlou, H. Adeli, and A. Adeli, "Improved visibility graph fractality with application for the diagnosis of autism spectrum disorder," *Phys. A, Statist. Mech. Appl.*, vol. 391, no. 20, pp. 4720–4726, 2012.
[4] Z. K. Gao, Q. Cai, Y. X. Yang, N. Dong, and S. S. Zhang, "Visibility graph from adaptive optimal kernel time-frequency representation for classification of epileptiform EEG," *Int. J. Neural Syst.*, vol. 27, no. 4, p. 1750005, Jun. 2017.
[5] S. Jiang, C. Bian, X. Ning, and Q. D. Y. Ma, "Visibility graph analysis on heartbeat dynamics of meditation training," *Appl. Phys. Lett.*, vol. 102, no. 25, p. 253702, 2013.
[6] I. Awan *et al.*, "Studying the dynamics of interbeat interval time series of healthy and congestive heart failure subjects using scale based symbolic entropy analysis," *PLoS ONE*, vol. 13, no. 5, p. e0196823, 2018.
[7] R. V. Donner, J. Heitzig, J. F. Donges, Y. Zou, N. Marwan, and J. Kurths, "The geometry of chaotic dynamics—A complex network perspective," *Eur. Phys. J. B*, vol. 84, no. 4, pp. 653–672, 2011.
[8] Z.-K. Gao, M. Small, and J. Kurths, "Complex network analysis of time series," *Europhys. Lett.*, vol. 116, no. 5, p. 50001, 2016.
[9] R. Flanagan and L. Lacasa, "Irreversibility of financial time series: A graph-theoretical approach," *Phys. Lett. A*, vol. 380, no. 20, pp. 1689–1697, 2016.
[10] Z.-K. Gao, X.-W. Zhang, N.-D. Jin, R. V. Donner, N. Marwan, and J. Kurths, "Recurrence networks from multivariate signals for uncovering dynamic transitions of horizontal oil-water stratified flows," *Europhys. Lett.*, vol. 103, no. 5, p. 50004, 2013.
[11] J. Zhang and M. Small, "Complex network from pseudoperiodic time series: Topology versus dynamics," *Phys. Rev. Lett.*, vol. 96, no. 23, p. 238701, 2006.
[12] Y. Yang and H. Yang, "Complex network-based time series analysis," *Phys. A, Stat. Mech. Appl.*, vol. 387, nos. 5–6, pp. 1381–1386, 2008.
[13] A. Nuñez, L. Lacasa, E. Valero, J. P. Gómez, and B. Luque, "Detecting series periodicity with horizontal visibility graphs," *Int. J. Bifurcation Chaos*, vol. 22, no. 7, p. 1250160, 2012.
[14] B. Luque, F. J. Ballesteros, A. Robledo, and L. Lacasa, "Entropy and renormalization in chaotic visibility graphs," in *Mathematical Foundations and Applications of Graph Entropy*, vol. 6. Hoboken, NJ, USA: Wiley, 2016, pp. 1–39. [Online]. Available: https://onlinelibrary.wiley.com/doi/book/10.1002/9783527693245
[15] Z. Gao and N. Jin, "Flow-pattern identification and nonlinear dynamics of gas-liquid two-phase flow in complex networks," *Phys. Rev. E, Stat. Phys. Plasmas Fluids Relat. Interdiscip. Top.*, vol. 79, no. 6, p. 66303, 2009.
[16] Z.-K. Gao, N.-D. Jin, W.-X. Wang, and Y.-C. Lai, "Motif distributions in phase-space networks for characterizing experimental two-phase flow patterns with chaotic features," *Phys. Rev. E, Stat. Phys. Plasmas Fluids Relat. Interdiscip. Top.*, vol. 82, no. 1, p. 16210, 2010.
[17] R. V. Donner, Y. Zou, J. F. Donges, N. Marwan, and J. Kurths, "Recurrence networks—A novel paradigm for nonlinear time series analysis," *New J. Phys.*, vol. 12, no. 3, p. 33025, 2010.
[18] L. Lacasa, B. Luque, F. Ballesteros, J. Luque, and J. C. Nuño, "From time series to complex networks: The visibility graph," *Proc. Nat. Acad. Sci. USA*, vol. 105, no. 13, pp. 4972–4975, 2008.
[19] B. Luque, L. Lacasa, F. Ballesteros, and J. Luque, "Horizontal visibility graphs: Exact results for random time series," *Phys. Rev. E, Stat. Phys. Plasmas Fluids Relat. Interdiscip. Top.*, vol. 80, no. 4, p. 46103, 2009.
[20] S.-D. Wu, C.-W. Wu, S.-G. Lin, K.-Y. Lee, and C.-K. Peng, "Analysis of complex time series using refined composite multiscale entropy," *Phys. Lett. A*, vol. 378, no. 20, pp. 1369–1374, 2014.
[21] J. S. Richman and J. R. Moorman, "Physiological time-series analysis using approximate entropy and sample entropy," *Amer. J. Physiol.-Heart Circulatory Physiol.*, vol. 278, no. 6, pp. H2039–H2049, 2000.
[22] C. Bandt and B. Pompe, "Permutation entropy: A natural complexity measure for time series," *Phys. Rev. Lett.*, vol. 88, no. 17, p. 174102, 2002.
[23] G. Manis, M. Aktaruzzaman, and R. Sassi, "Bubble entropy: An entropy almost free of parameters," *IEEE Trans. Biomed. Eng.*, vol. 64, no. 11, pp. 2711–2718, Nov. 2017.
[24] J. Iacovacci and L. Lacasa, "Sequential motif profile of natural visibility graphs," *Phys. Rev. E, Stat. Phys. Plasmas Fluids Relat. Interdiscip. Top.*, vol. 94, no. 5, p. 52309, 2016.

[25] C. E. Shannon, "A mathematical theory of communication," *Bell Syst. Tech. J.*, vol. 27, no. 3, pp. 623–656, Jul./Oct. 1948.
[26] M. Costa, A. L. Goldberger, and C.-K. Peng, "Multiscale entropy analysis of complex physiologic time series," *Phys. Rev. Lett.*, vol. 89, no. 6, p. 68102, 2002.
[27] M. Costa, A. L. Goldberger, and C.-K. Peng, "Multiscale entropy analysis of biological signals," *Phys. Rev. E, Stat. Phys. Plasmas Fluids Relat. Interdiscip. Top.*, vol. 71, no. 2, p. 21906, 2005.
[28] E. Sejdić and L. A. Lipsitz, "Necessity of noise in physiology and medicine," *Comput. Methods Programs Biomed.*, vol. 111, no. 2, pp. 459–470, Aug. 2013.
[29] L. Lacasa, "Horizontal visibility graphs from integer sequences," *J. Phys. A, Math. Theor.*, vol. 49, no. 35, p. 35LT01, 2016.
[30] PhysioNet. *PhysioNet is supported by the National Institute of General Medical Sciences (NIGMS)*. Accessed: Feb. 4, 2017. [Online]. Available: https://www.physionet.org/
[31] American Heart Association (AHA). *Classes of Heart Failure*. Accessed: Sep. 15, 2016. [Online]. Available: http://www.heart.org/HEARTORG/Conditions/HeartFailure/AboutHeartFailure/Classes-of-Heart-Failure_UCM_306328_Article.jsp#.WfOkMWiCxPY
[32] W. Aziz, M. Rafique, I. Ahmad, M. Arif, N. Habib, and M. S. Nadeem, "Classification of heart rate signals of healthy and pathological subjects using threshold based symbolic entropy," *Acta Biologica Hungarica*, vol. 65, no. 3, pp. 252–264, 2014.
[33] M. Costa, A. L. Goldberger, and C.-K. Peng, "Multiscale entropy analysis of biological signals," *Phys. Rev. E, Stat. Phys. Plasmas Fluids Relat. Interdiscip. Top.*, vol. 71, no. 2, p. 21906, 2005.
[34] J. Iacovacci and L. Lacasa, "Sequential visibility-graph motifs," *Phys. Rev. E, Stat. Phys. Plasmas Fluids Relat. Interdiscip. Top.*, vol. 93, no. 4, p. 42309, 2016.

GULRAIZ IQBAL CHOUDHARY received the master's degree in software technology from Linnaeus University, Vaxjo, Sweden, in 2009, and the master's degree in computer science from Mohi-ud-Din Islamic University, Islamabad, Pakistan, in 2004. He is currently pursuing the Ph.D. degree with the School of Computing, University of Eastern Finland, Joensuu, Finland. His research interests include biomedical signal processing, complex networks, nonlinear time series analysis, image processing, machine learning, and computer vision.

WAJID AZIZ was born in Azad Kashmir, Pakistan, in 1970. He received the M.Sc. degree in physics from the University of Azad Jammu & Kashmir (AJ&K), the Ph.D. degree in computer and information sciences from the Pakistan Institute of Engineering and Applied Sciences, Islamabad, Pakistan, in 2006, and the Ph.D. degree from the University of Leicester, U.K., in 2011. He served at the University of AJ&K in various capacities. He is currently a Professor with the Faculty of Computing and Information Technology, University of Jeddah. He has collaborated actively with researchers in several other disciplines of computing and information technology. His research interests include biomedical signal processing, data mining and machine learning, and nonlinear time series analysis.

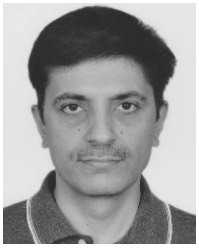

ISHTIAQ RASOOL KHAN received the B.Sc. degree in electrical engineering from the University of Engineering and Technology, Taxila, Pakistan, in 1992, the M.S. degree in systems engineering from Quaid-i-Azam University, Islamabad, Pakistan, in 1994, and the M.S. degree in information engineering and the Ph.D. degree in digital signal processing from Hokkaido University, Japan, in 1998 and 2000, respectively, where he was a JSPS Fellow, from 2000 to 2002. He was with the University of Kitakyushu, Japan, the Kyushu Institute of Technology, Japan, and the Institute for Infocomm Research, A*STAR, Singapore in the past. He is currently a Professor with the Faculty of Computing and Information Technology, University of Jeddah. His research interests include high dynamic range imaging, data analytics, and digital filtering.

SUSANTO RAHARDJA (F'11) is currently a Chair Professor with Northwestern Polytechnical University under the Thousand Talent Plan of China. He contributed to the development of a series of audio compression technologies, such as Audio Video Standards AVS-L, AVS-2, ISO/IEC 14496-3:2005/Amd.2:2006, and ISO/IEC 14496-3:2005/Amd.3:2006, in which some have been licensed to several companies. He has more than 15 years of experience in leading research team for media-related research that cover areas in signal processing (audio coding and video/image processing), media analysis (text/speech, image, and video), media security (biometrics, computer vision, and surveillance), and sensor networks. He has published more than 300 papers. His research interests include multimedia, signal processing, wireless communications, discrete transforms, and signal processing algorithms and implementation.

Dr. Rahardja was a recipient of several honors, including the IEE Hartree Premium Award, the Tan Kah Kee Young Inventors' Open Category Gold Award, the Singapore National Technology Award, the A*STAR Most Inspiring Mentor Award, the Finalist of the 2010 World Technology and Summit Award, the Nokia Foundation Visiting Professor Award, and the ACM Recognition of Service Award. He was the Conference Chair of the 5th ACM SIGGRAPHASIA, in 2012, and the APSIPA 2nd Summit and Conference, in 2010 and 2018, as well as other conferences in the ACM, the SPIE, and the IEEE. He was an Associate Editor of the IEEE Transactions on Audio, Speech and Language Processing and the IEEE Transactions on Multimedia and a Senior Editor of the IEEE Journal of Selected Topics in Signal Processing, and is currently serving as an Associate Editor for the *Elsevier Journal of Visual Communication and Image Representation* and the IEEE Transactions on Multimedia.

He received the B.Eng. degree from the National University of Singapore and the M.Eng. and Ph.D. degrees in electronic engineering from Nanyang Technological University, Singapore. He attended the Stanford Executive Programme at the Graduate School of Business, Stanford University, USA.

PASI FRÄNTI received the M.Sc. and Ph.D. degrees in science from the University of Turku, in 1991 and 1994, respectively. Since 2000, he has been a Professor of computer science with the University of Eastern Finland. He has published 78 journals and 167 peer review conference papers, including 14 IEEE transaction papers. Significant contributions have also been made in image compression, image analysis, vector quantization, and speech technology. His main research interests include machine learning, data mining, and pattern recognition, including clustering algorithms and intelligent location-aware systems.